

Solid Surface Combustion Experiment  
Flame Spread in a Quiescent, Microgravity Environment  
Implications of Spread Rate and Flame Structure

Matthew Bundy, Jeff West, Peter C. Thomas, and Subrata Bhattacharjee  
Department of Mechanical Engineering  
San Diego State University, San Diego, CA 92182-0191

Lin Tang and Robert A. Altenkirch  
Department of Mechanical Engineering and  
NSF Engineering Research Center for Computational Field Simulation  
Mississippi State University, Mississippi State, MS 39762

and  
Kurt Sacksteder  
NASA Lewis Research Center  
Cleveland, OH 44135

**Introduction:**

A unique environment in which flame spreading, a phenomenon of fundamental, scientific interest, has importance to fire safety is that of spacecraft in which the gravitational acceleration is low compared with that of the Earth, i.e., microgravity. Experiments aboard eight Space Shuttle missions between October 1990 and February 1995 were conducted using the Solid Surface Combustion Experiment (SSCE) payload apparatus in an effort to determine the mechanisms of gas-phase flame spread over solid fuel surfaces in the absence of any buoyancy induced or externally imposed oxidizer flow. The overall SSCE effort began in December of 1984.

The SSCE apparatus consists of a sealed container, approximately  $0.039 \text{ m}^3$ , that is filled with a specified  $\text{O}_2 / \text{N}_2$  mixture at a prescribed pressure. Five of the experiments used a thin cellulosic fuel, ashless filter paper, 3 cm wide by 10 cm long, 0.00825 cm half-thickness, ignited in five different ambient conditions. Three of the experiments, the most recent, used thick polymethylmethacrylate (PMMA) samples 0.635 cm wide by 2 cm long, 0.32 cm half-thickness. Three experiments, STS 41, 40 and 43, were designed to evaluate the effect of ambient pressure on flame spread over the thin cellulosic fuel while flights STS 50 and 47 were at the same pressure as two of the earlier flights but at a lower oxygen concentration in order to evaluate the effect of ambient oxygen level on the flame spread process at microgravity. For the PMMA flights, two experiments, STS 54 and 63, were at the same pressure but different oxygen concentrations while STS 64 was at the same oxygen concentration as STS 63 but at a higher pressure.

Two orthogonal views of the experiments were recorded on 16 mm cine-cameras operating at 24 frames/s. In addition to filmed images of the side view of the flames and surface view of the burning samples, solid- and gas-phase temperatures were recorded using thermocouples. The experiment is battery powered and follows an automated sequence upon activation by the Shuttle Crew.

In this study we separate the SSCE data into two groups according to the fuel type: i) thin cellulose, and ii) thick PMMA. The experimental spread rates are compared with prediction from a number of models in an effort to uncover the important physics that characterize microgravity flame spread. Both steady and unsteady solutions are employed to explore the flame evolution, especially for thick fuels. Finally, the flame structure in downward spread is compared with the microgravity flame structure and modeling results to delineate the difference between the two configurations and the influence of normal gravity.

**Mathematical Model:**

The mathematical model employed has been reported before [1], so only a brief description is presented here. The conservation equations can be expressed in a generic format as follows:

$$\frac{\partial(\rho\phi)}{\partial t} + \frac{\partial(\rho u\phi)}{\partial x} + \frac{\partial(\rho v\phi)}{\partial y} = \frac{\partial}{\partial x} \left\{ \Gamma_{\phi} \frac{\partial\phi}{\partial x} \right\} + \frac{\partial}{\partial y} \left\{ \Gamma_{\phi} \frac{\partial\phi}{\partial y} \right\} + \dot{s}_{\phi}''' \quad (1)$$

where the terms are explained in Table 1. The ignition source term applies only to the shaded ignition zone of Fig. 1. The Planck mean absorption coefficient,  $a_{p,GB}$ , calculated from the method of Global Energy Balance [2], accounts for reabsorption of radiation despite the apparent thin optical limit of the radiation source term.

In addition to the conservation equations, the equations of state for density, viscosity and thermal conductivity in the gas phase, a pyrolysis formula based on negligible surface regression and constant solid density for the thick fuel, and variable density and first-order kinetics for the thin fuel are used to complete the formulation.

$$\rho = \frac{P_\infty M_\infty}{RT}; \quad \frac{\mu}{\mu_r} = \frac{\lambda}{\lambda_r} = \sqrt{\frac{T}{T_r}}; \quad \dot{m}''_{thin} = B_p \rho_s \tau \exp\left(-\frac{T_{a,p}}{T_s}\right);$$

$$\dot{m}''_{thick} = \left\{ \frac{\rho_s T_s^2 B_p \lambda_s}{T_{a,p} [3.615 \Delta h_v^o + 4.605 c_s (T_s - T_\infty)]} \right\}^{1/2} \exp\left(-\frac{T_{a,p}}{2T_s}\right) \quad (2)$$

The boundary conditions are depicted in Fig. 1. The properties used for thick and thin fuels are:  $s = 1.92, 1.185$ ;  $\Delta h_c^o = 25.9, 16.74$  MJ / kg<sub>fuel</sub>;  $B_c = 5.928 \times 10^9, 1.58 \times 10^{11}$  m<sup>3</sup> / kg · s;  $T_{a,c} = 10.7, 14.04$  kK;  $c_g = 1.183, 1.465$  kJ / kg · K;  $\lambda_r = 0.086$  W / m · K;  $\mu_r = 0.675 \times 10^{-3}$  N · s / m<sup>2</sup>;  $T_r = \frac{T_\infty + T_{ad}}{2} = 1958$  K;  $M_\infty = 30$  kg / kmol;  $c_s = 1.465, 1.256$  kJ / kg · K;  $\Delta h_v^o = 0.941, 0.368$  MJ / kg<sub>fuel</sub>;  $\lambda_s = 0.035, 0.12$  W / m · K;  $\rho_s = 1190, 518.7$  kg / m<sup>3</sup>;  $\tau = 3.2, 0.083$  mm;  $B_p = 2.282 \times 10^9, 7.8 \times 10^{16}$  s<sup>-1</sup>;  $T_{a,p} = 15.6, 30.0$  kK. The boundary conditions and typical numerical parameters are:  $y_{O,\infty} = 0.53$ ;  $P_\infty = 1$  atm;  $V_g = 0$  or 1 cm/s;  $y_{max} = 100$  mm;  $y_{min} = 3.2$  mm;  $x_{max} - x_{min} = 200$  mm; Number of grid points 37x90; the time step ranges from 0.01 s to 0.25 s. The ignition volume ( $\Delta V_{ign}$ ) is  $1.6 \times 1.6 \times 6.3$  mm<sup>3</sup> in each phase.

## Results and Discussion:

### 1. Thin Fuel:

**1.1 Spread Rate:** The experimental flame spread rates,  $V_{f,exp}$ , over the thin cellulosic fuel in five different quiescent environments, at three different ambient pressures and two oxygen levels, are plotted in Fig. 2. Superposed on this figure is the prediction from the de Ris theory [3],  $V_{f,deRis}$ , the prediction from a non-radiative computational model similar to that of Frey and T'ien [4],  $V_{f,non-rad}$ , and, the prediction from a radiative model [5]. The non-radiative models over-predict  $V_f$  by almost a factor of 2 to 3. Moreover, the clear trend seen in the experiments, an increase in  $V_f$  with  $P_\infty$ , is completely missed by these models. The model with radiation produces the best agreement (within 10%) with experiment.

The near-perfect agreement between the de Ris formula and the non-radiative model needs some explanation. The spread rate is computed using a succession of models in which the major assumptions in the de Ris theory - zero hang-distance (#2), Oseen flow (#3), constant gas density (#4), no wall blowing (#5), infinite-rate chemistry (#6), constant vaporization temperature (#7), constant solid density (#8), constant gas conductivity (#9), and no radiation (#10-#13) - are removed one by one, and the resulting spread rates are plotted in Fig. 3 for two ambient pressures and two  $V_g$ 's. On the very left of the abscissa is the prediction from the de Ris formula (#1), and on the extreme right are the data (#14) from the SSCE and literature [6] with the intermediate points being the various mathematical models with increasing complexity. It is clear from this figure that many of the assumptions in the de Ris theory have a canceling affect, and that is why the non-radiative model (#9) produces the same spread rate as the de Ris formula (#1).

Results from four different radiative models (#10: surface re-radiation only; #11: gas radiation only; #12: surface and gas radiation loss; #13: surface and gas radiation with radiation feedback from gas to solid) are also shown in

Fig. 3. With the inclusion of any sort of radiative mechanism,  $V_f$  shows a significant decrease, and the observed behavior of  $V_f$  with  $P_\infty$  is qualitatively reproduced. It is also evident that the radiative effects on spread rate decrease as the ambient pressure is reduced or  $V_g$  is increased.

**1.2 Flame Structure:** Photographs showing the side view of the flame at two different pressures are shown in Figs. 4(a) and 4(b) (see color appendix). Temperature recorded by a thermocouple embedded in the solid and a gas-phase thermocouple 7 mm above the surface are superposed on these photos after converting time into distance assuming the flame to be steady. At higher pressure, the presence of bright soot near the leading edge makes it impossible for the photograph to capture the entire flame image. At 1.0 atm, the flame length seems to correspond to the distance between the two peaks shown by the gas-phase thermocouple. If this is also true at 1.5 atm, the flame size must increase with the ambient pressure, a conclusion predicted from the model with radiation [5].

Another feature that is immediately noticeable in Fig. 4 is the presence of a large, 10 mm long hang-distance [7], the distance between the flame leading edge and the pyrolysis front, with the latter location identified by the surface temperature reaching a plateau following the preheat region. Contrast these flame pictures with that of a downward spreading flame at 1-g shown in Fig. 5. The flame size as well as the hang-distance is much smaller at 1-g because the diffusion length,  $L_g \equiv \frac{\alpha_g}{(V_g + V_f)}$ , is only about 0.158 cm ( $V_g \approx 20$  cm/s) as opposed to 11.1 cm in the quiescent, microgravity environment.

The dependence of vaporization temperature on pressure and the velocity scale in Figs. 4 and 5 can be qualitatively explained from the correlation developed by Bhattacharjee et al. [8]. The presence of soot in Figs. 4(b) and 5 can be qualitatively explained by the smaller residence time,  $t_{res} = \frac{L_g}{(V_g + V_f)}$ , at higher  $P_\infty$  or  $V_g$ .

## 2. Thick Fuel:

**2.1 Ignition Transient for Thick Fuel:** For thick PMMA, the ignition transient is more prominent than in the case of the thin cellulosic fuel; it can be divided into the following sequence of events: i) preheating, ii) premixing, iii) ignition, iv) premixed flame propagation, and v) reverse flame propagation. The premixed flame propagation is captured by the unsteady model. The gas-phase thermocouple data, with the thermocouple fixed at  $x = 10$  mm,  $y = 1$  mm, shows an initial spike at around  $t=5$  s (see Fig. 6) as the premixed flame approaches the thermocouple, stops at  $x=6$  mm, and then retreats back to  $x=3$  mm. The temperature starts rising again as the stabilized spreading flame arrives. The premixed propagation phase has been computationally found to last for a shorter duration with a decrease in  $E_{ign}$  and can be completely absent as in the case of thin fuels. The latter conclusion is supported by the lack of the initial spike in the gas-phase thermocouple traces of Fig. 4.

**2.2 Unsteady Flame Spread:** After the ignition transient is over, the flame, still very small in size, starts spreading in the x-direction. Computed and experimental  $V_f$ , plotted against  $x$  in Fig. 7, decrease smoothly, and extinction results at high values of  $x$ . The steady code also predicts a zero value for  $V_f$  as does the de Ris formula. In the experiments, the spread rate decreases with  $x$ ; however, self extinguishment was not observed, perhaps because of the short length of fuel over which the spread occurred.

The time of extinction for different ambient conditions in Fig. 7 can be explained if the diffusion time scale,

$t_{diff} \approx \frac{L^2}{\alpha_g}$ , is obtained from a fixed imposed length. As pressure is doubled, so is  $t_{diff}$ , which may explain why the

50%, 2 atm flame lasts almost twice as long as the 50%, 1 atm flame. The time scale is almost independent of  $O_2$  level; however, because of the higher  $O_2$  level at  $t=0$ , it takes longer for the near-limit condition to be reached at higher  $O_2$  level.

## Conclusions:

Experimental results from the SSCE and computational results from steady and unsteady modeling are presented. It is established that for thin cellulosic fuel the flame spread phenomenon is fairly steady after the initial ignition transients are over. The flame size and the hang distance are much larger in microgravity than in downward flame propagation. The fundamental mechanism behind the striking differences between the 0-g and 1-g flame seems to be the enhancement of radiation heat transfer in the quiescent, microgravity environment because of the large residence time. For thick fuels, a premixed flame propagation during ignition has been captured by the unsteady model as well as the experiments. The models also indicate that the flame spreads with a decreasing spread rate and finally may extinguish even at high oxygen levels.

**Acknowledgments:** This work was supported by NASA through Contract NAS3-23901.

## References:

1. Bullard, D.B., Tang, L., Altenkirch, R.A., and Bhattacharjee S., *Finite-Rate Chemistry in Unsteady Flame Spread Over Solid Fuels in Microgravity*, Adv. Space Research, Vol. 13, No. 7, pp.(7)171-(7)184, (1993).
2. Bhattacharjee, S., and Altenkirch, R.A., *Radiation- Controlled, Opposed-Flow Flame Spread in a Microgravity Environment*, Twenty-Third Symp. (Int.) on Comb., The Comb. Inst., Pittsburgh, pp. 1627-1633, (1990).
3. de Ris, J.N., *Spread of a Laminar Diffusion Flame*, Twelfth Symp. (Int.) on Comb., The Comb. Inst., Pittsburgh, PA, p. 241, (1969).
4. Frey, A.E., and T'ien, J.S., *A Theory of Flame Spread over a Solid Fuel Including Finite-Rate Chemical Kinetics*, Combustion and Flame, Vol. 36, pp. 263-289, (1979).
5. Bhattacharjee, S., Altenkirch, R.A., and Sacksteder, K., *The Effect of Ambient Pressure on Flame Spread Over Thin Cellulosic Fuels in a Quiescent, Microgravity Environment*, Journal of Heat Transfer, To Appear, (1995).
6. Fernandez-Pello, A.C., Ray, S.R., and Glassman, I., *Flame Spread in an Opposed Forced Flow: The Effect of Ambient Oxygen Concentration*, Eighteenth Symp. (Int.) on Comb., The Comb. Inst., Pittsburgh, PA, p. 579, (1981).
7. Bhattacharjee, S., West, J., and Dockter, S., *A Simplified Theory for de Ris Flame over Thin and Thick Fuels*, Combustion and Flame, Accepted, (1995).
8. Bhattacharjee, S., Bhaskaran, K.K., and Altenkirch, R.A., *Effects of Pyrolysis Kinetics on Opposed Flow Flame-spread Modeling*, Combustion Science and Technology, Vol. 100, pp. 163-183, (1994).

Equation	$\phi$	$\Gamma_\phi$	$\dot{s}_\phi'''$
Mass	1	0	0
x-mom.	u	$\mu$	$-\frac{\partial P}{\partial x}$
y-mom.	v	$\mu$	$-\frac{\partial P}{\partial y}$
Species: Fuel	$y_F$	$\lambda / c_p$	$-B_c \rho_s^2 y_F y_O \exp\left\{-\frac{T_{a,c}}{T}\right\}$
Species: Oxygen	$y_O$	$\lambda / c_p$	$s \dot{s}_F'''$
Species: Nitrogen	$y_N$	$\lambda / c_p$	0
Energy: Gas-Phase	T	$\lambda / c_p$	$\frac{\Delta \dot{h}_c^o \dot{s}_F''' + \dot{q}_{ign}'''}{c_p} - 4a_{p,GB}(T^4 - T_\infty^4)$
Energy: Solid-Phase	$T_s$	$\lambda / c_p$	$\frac{\dot{q}_{ign}'''}{c_s}$

Table 1. Description of the generic terms of Eq. (1).

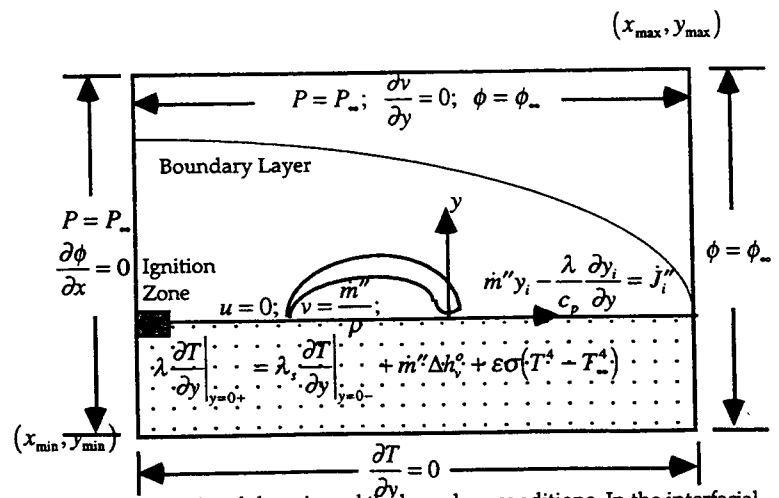


Fig. 1. Computational domain and the boundary conditions. In the interfacial species continuity equation  $J_i'' = m''$  for fuel, and  $J_i'' = 0$  for others.

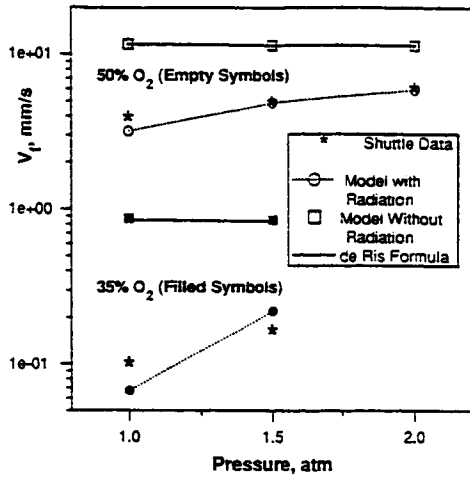


Fig. 2.  $V_f$  vs.  $P_\infty$  at two different  $O_2$  levels. Data from Space Shuttle experiments, predictions of the de Ris formula, and models with and without radiation.

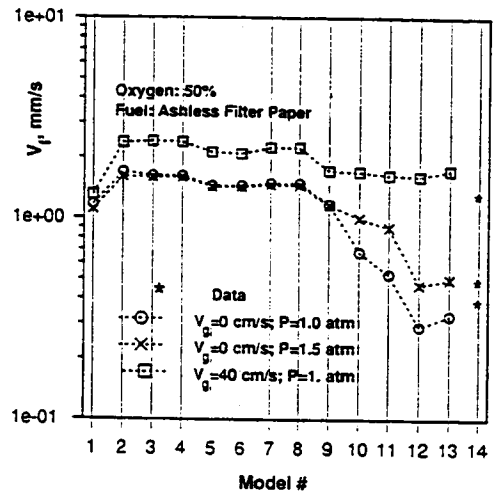


Fig. 3. Model sweep for spread rate. On the left is the de Ris model and on the right are data from the Space Shuttle experiments and literature [6] with intermediate models removing the assumptions in the de Ris theory one by one.

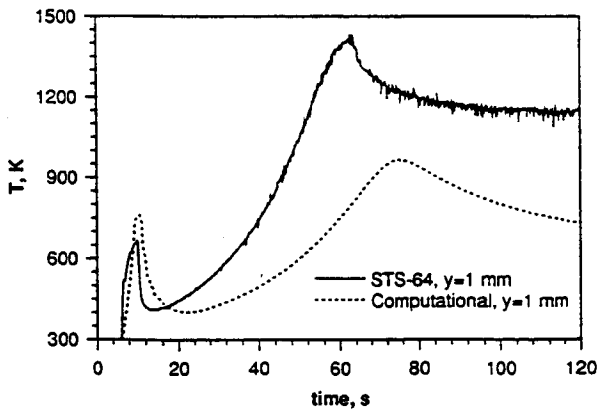


Fig. 6. Temperature recorded by a thermocouple 1 mm away from the surface in flame spread over PMMA. The initial temperature spikes in the Shuttle data (solid line) and the unsteady theory indicate the propagation of a premixed flame during the ignition transient.

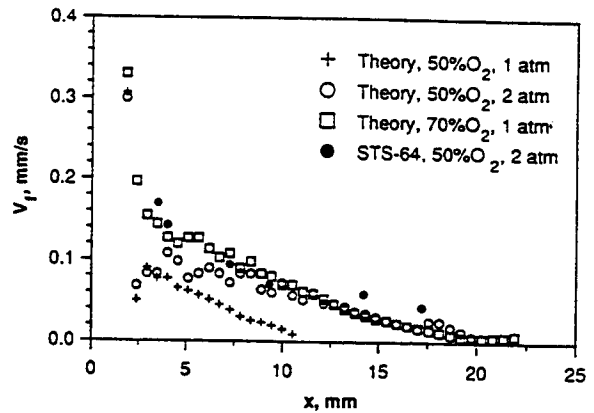
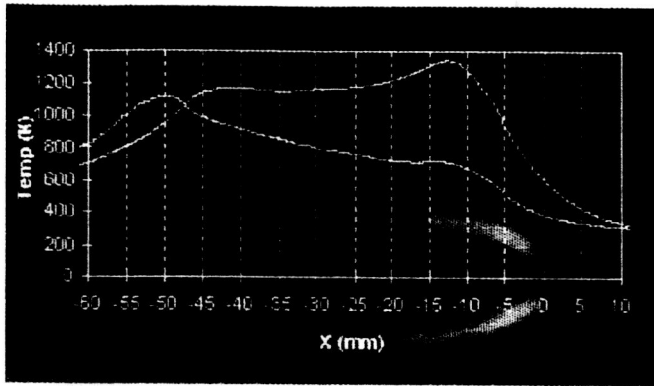
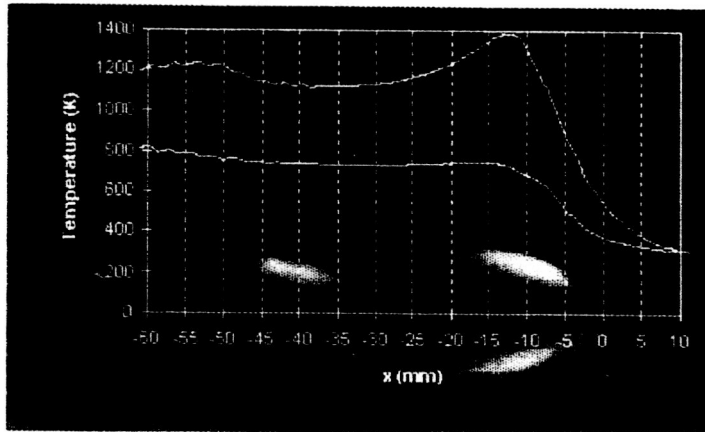


Fig. 7. Unsteady computations of  $V_f$  over PMMA for three different ambient conditions showing eventual extinguishment.



(a)



(b)

Fig. 4. Visual side view of the flame spreading over thin fuel at 50%  $O_2$ , and, a)  $P_\infty = 1.0$  atm, b)  $P_\infty = 1.5$  atm. Superposed are the thermocouple traces, one embedded in the solid and the other in the gas phase, 7 mm away from the surface.

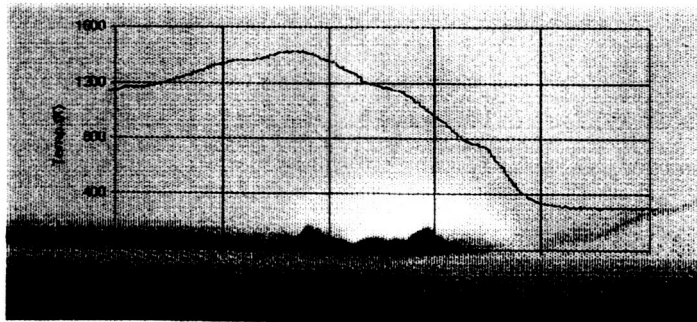


Fig. 5. Visual side view of a downward spreading flame over Ashless Filter Paper at 21%  $O_2$ ,  $P_\infty = 1.0$  atm. Superposed is the surface thermocouple trace.

**Solid Surface  
Combustion Experiment**

ORIGINAL PAGE  
COLOR PHOTOGRAPH